Population Balance Model for Emulsion Polymerisation Under Pseudo-Bulk Conditions: Combined Particle Size Distribution and Molecular Weight Distribution

Stephen J. Sweetman,[1] *Charles D. Immanuel,**[1] *Tahir Malik,*[2] *Simon Emmett,*[3] *Neal Williams*[3]

Summary: A comprehensive model for emulsion polymerisation is presented, accounting for particle size distribution (PSD) and molecular weight distribution (MWD). The PSD information is incorporated through a population balance framework. A mechanistic formulation is adopted in modelling the average number of radicals/particle under pseudo-bulk compartmentalisation conditions. The method of moments is adopted to simplify the MWD equations over each discrete size class. The impact of the pseudo-bulk assumption on the PSD and MWD results is assessed. An identification of potential manipulated variables for control of PSD and MWD is done through sensitivity analysis.

Keywords: combined MWD and PSD; emulsion polymerisation; population balance model; pseudo-bulk conditions

1 Introduction

Emulsion polymerisation represents a classical problem in distribution control and multi-objective control. The effect of the particle size distribution (PSD) on end-use properties such as rheology is well known.[1,2] In addition, the molecular weight distribution (MWD) influences end-use properties such as mechanical strength[3] and the fourth moment of MWD is expected to be correlated with the rheology.[4] Thus, the control of PSD and MWD represents an inferential control of end-use properties of the emulsion polymer, and underlines the importance of a detailed mathematical model for PSD and MWD.

The first mathematical models based on the Harkins framework were developed by Smith and Ewart.[5] Certain limiting cases were identified; one wherein the average number of radicals per particle was small ($\overline{n} \ll 0.5$), another wherein $\overline{n}$ was approximately equal to 0.5 (zero-one system) and a third wherein $\overline{n}$ was large compared to unity (pseudo-bulk system). The literature reports a plethora of valuable contributions to model the emulsion polymerisation process. These include detailed models for PSD[6–21] which can be classified into two main classes. The first class is the so-called pseudo-bulk models that address the third limiting case ($\overline{n} \gg 1$), and the second is the so-called zero-one models that address the other limiting cases.

Parallel to the development of PSD models, the literature presents comprehensive developments of MWD models.[6,12,18,22–27] A key issue to consider in this context is the compartmentalisation of the radicals among the particles i.e. a radical in one particle cannot terminate with a radical in another particle. Based on

[1] Centre for Process Systems Engineering, Imperial College London SW7 2AZ, UK
[2] ICI Strategic Technology Group, Wilton Centre, UK
[3] ICI Paints, Slough, UK

the concept of the singly and doubly distinguished particle,[28] Ghielmi et al.[29] and Butte et al.[30] developed models for MWD by considering a particle population of the form $N_{i,m,n}$, which represents doubly distinguished particles with i radicals, containing a pair of radicals with chain lengths n and m. It was shown that significant errors in MWD estimation could be made in neglecting the compartmentalisation phenomenon. This effect was particularly apparent when the number of radicals per particle was small (i.e. $\overline{n} < 1$). Arzamendi et al.[26] also found that in their model based on the so-called partial distinction approach, the predicted MWD was erroneous under conditions where $\overline{n}$ was small.

Min and Ray[6] developed the first comprehensive model for PSD and MWD employing a population balance equation (PBE) framework. Later Saldivar et al.[12] extended this model to copolymer systems based on an exhaustive kinetic scheme. More recently Park et al.[31] formulated and solved a comprehensive model for PSD and MWD for a realistic copolymerisation system. Reynhout et al.[32] introduce a correction factor to account for the compartmentalisation issue in their comprehensive model.

In this article, a combined model for PSD and MWD is presented. As will be shown, the system studied exhibits a highly pseudo-bulk character for a majority of the operating regime. Although the model does not specifically account for effect of compartmentalisation on the termination rates, a study of the sensitivity of the model results to this approximation is presented.

2 Comprehensive Model Formulation

2.1 Particle Size Distribution

The population balance equation provides the ideal framework to model the PSD and MWD in emulsion polymerisation.[6] The PSD is described by the PBE (equation (1)) that accounts for particle nucleation, particle growth and inter-particle coagulation:

$$\frac{\partial}{\partial t}F(r,t) + \frac{\partial}{\partial r}\left(F(r,t)\frac{dr}{dt}\right) = \Re_{nuc}(r,t) + \Re_{coag}(r,t) \quad (1)$$

Here the particle density $F(r,t)dr$ is defined as the moles of particles of unswollen size between r and $r+dr$ at time t. The growth rate dr/dt is related to the rate of polymerisation within the particles. The nucleation rate $\Re_{nuc}$ accounts for both micellar and homogenous nucleation (details can be found in the paper by Immanuel et al.[33]) The coagulative-nucleation phenomenon is assumed to be negligible. Inter-particle coagulation is modelled under ionic stabilisation by surfactants.[11,34,35]

Although the pseudo-bulk framework is adopted in this work, a first principles approach based on a balance between the rates of entry, desorption and termination of radicals in particles is employed in modelling $\overline{n}(r,t)$ as shown in equation (2):

$$\frac{\partial \overline{n}}{\partial t}(r,t) = \Re_{entry}(r) - \Re_{desorp}(r) - 2\Re_{termin}(r) \quad (2)$$

Here $\Re_{entry}$ is the total rate of entry into a single particle of size r, $\Re_{desorp}$ is the total rate of desorption from a single particle of size r and $\Re_{termin}$ is the total rate of termination within a single particle of size r. A pseudo steady state is assumed for equation (2). The global average can be derived from $\overline{n}$ by equation (3):

$$\overline{n}_{global} = \frac{\int_{r\min}^{r\max} \overline{n}(r,t)F(r,t)dr}{\int_{r\min}^{r\max} F(r,t)dr} \quad (3)$$

2.2 Molecular Weight Distribution

Population balances are formulated for the live and dead polymer population chain length distribution as follows.[12,31] The main assumptions that have been made in the MWD model include insensitivity of the MWD to the coagulation phenomenon [31]

and the general validity of pseudo-bulk conditions. The live polymer population, $N^l(r,t)$ is defined as the concentration of radicals (in mol/litre) of length l in a particle of size r at time t, given by equations (4), (5) and (6):

$$\begin{aligned}\frac{\partial}{\partial t}N^0(r,t) &= \sum_{i=1}^{2} e_i^0 Pwi[P_w^0]/V_p N_A \\ &\quad - \overline{k}_p[M_{pj}]N^0 + \overline{k}_{tr}[M_{pj}](\overline{n}-N^0) \\ &\quad + \overline{k}_{trcta}[CTA_p](\overline{n}-N^0) - \overline{k}_t\overline{n}N^0 \\ &\quad - \sum_{j=1}^{2} k_{dnjPj}N^0 \end{aligned} \tag{4}$$

$$\begin{aligned}\frac{\partial}{\partial t}N^l(r,t) &= \sum_{i=1}^{2} e_i^l Pwi[P_w^l]/V_p N_A + \overline{k}_p[M_{pj}] \\ &\quad \times (N^{l-1}-N^l) - \overline{k}_{tr}[M_{pj}]N^l \\ &\quad - \overline{k}_{trcta}[CTA_p]N^l - \overline{k}_t\overline{n}N^l \\ &\quad (1 \le l < j_{cr})\end{aligned} \tag{5}$$

$$\begin{aligned}\frac{\partial}{\partial t}N^l(r,t) &= +\overline{k}_p[M_{pj}](N^{l-1}-N^l) \\ &\quad - \overline{k}_{tr}[M_{pj}]N^l - \overline{k}_{trcta}[CTA_p]N^l \\ &\quad - \overline{k}_t\overline{n}N^l \\ &\quad (j_{cr} \le l < \infty))\end{aligned} \tag{6}$$

The first term on the right of equation (4) accounts for the entry of an oligomer of length 0 (monomeric radical derived from chain transfer to monomer) from the aqueous phase into particle of size r. The second term accounts for loss of monomeric radicals from a particle of size r when a monomeric radical propagates with a monomer unit to form a radical of length 1. The third and fourth terms account for the chain transfer reactions to both monomer and to chain transfer agent (CTA) in a particle of size r. The term '$-N^0$' accounts for the net cancelation of the effect of chain transfer to a monomeric radical on the number of monomeric radicals. The fifth term on the right of equation (4) accounts for termination reactions, whereby a monomeric radical can terminate with any length radical in a particle of size r (negative contribution to N^0 balance). The final term accounts for desorption of monomeric radicals from a particle of size r. Note that only the monomeric radicals are considered to desorb. The aqueous phase radicals contain an initiator derived ionic charge. However, radicals inside particles are primarily derived from monomer and have no charge, therefore are less likely to desorb. Also the live radical population in a particle is very small compared to the dead polymer so the effect of this assumption will be minimal. j_{cr} is the critical chain length of aqueous phase oligomers, representing the aqueous phase solubility limit, beyond which homogenous nucleation occurs. Thus, no radicals with chain length beyond $j_{cr}-1$ are found in the aqueous phase, accounting for the absence of the entry term in equation (6). The notation e_i^l is the rate of entry into a particle of a radical of type i and length l, $[P_w^l]$ is the concentration of oligomers of length l in the aqueous phase, N_A is the Avogadro constant, $[\mathrm{CTA_p}]$ is the concentration of CTA in the particle phase, $[M_p]$ is the concentration of monomer in the particle phase, k_{dnj} is the desorption rate constant for a monomeric radical of type j, p_i is the pseudo-homopolymer probability of finding a radical with an end unit of type i in the particle phase and p_{wi} is the pseudo-homopolymer probability of finding a radical with an end unit of type i in the aqueous phase. Note that when applied to the aqueous phase radicals the pseudo-homopolymer probability could be of reduced applicability in view of the short chain lengths of these radicals. However, the overall sensitivity of the model predictions to the aqueous phase radicals is minimal and this assumption is found to be valid in previous publications.[33] $\overline{k}_p$, $\overline{k}_{tr}$, $\overline{k}_{trcta}$, $\overline{k}_t$, $\overline{k}_{tc}$, $\overline{k}_{td}$ are the pseudo-homopolymer rate constants for propagation, chain transfer to monomer, chain transfer to CTA,

total termination, termination by combination and termination by disproportionation, respectively (see[33] for further details).

The dead chain population is defined as the concentration (mol/litre) of polymer chains of length l in a particle of size r at time t, given in equation (7):

$$\frac{\partial}{\partial t}D^l(r,t) = \overline{k}_{tr}[M_{pj}]N^l + \overline{k}_{trcta}[CTA_p]N^l + \overline{k}_{td}\overline{n}N^l + \sum_{i=1}^{2}\sum_{j=1}^{2}\frac{\overline{k}_{tc}}{2}\sum_{m=0}^{l}N^m N^{l-m} \quad (7)$$

In equation (7), the first two terms account for chain transfer to monomer and CTA respectively, and the last two terms account for termination reactions by disproportionation and combination respectively.

2.3 Method of Moments for MWD

The solution of the combined PSD and MWD model presented in Sections 2.1 and 2.2 is highly computation-intensive. In order to facilitate computation, the method of moments is adopted to simplify the live and dead chain length distribution. Thus, the k^{th} moment of the live and dead chains inside particles of size r is defined, respectively, by equations (8) and (9)

$$\lambda_{Nk} = \sum_{l=0}^{\infty} l^k\left(N^l(r,t)\right) \quad (8)$$

$$\lambda_{Dk} = \sum_{l=0}^{\infty} l^k(D^l(r,t)) \quad (9)$$

The zeroth moment of the live radical population is linearly related to the average number of radicals/particle, $\overline{n}$. Thus, the zeroth moment in a particle of size r at time t is defined as in equation (10):

$$\lambda_{N0}(r,t) = \overline{n}(r,t)/V_pN_A \quad (10)$$

Here V_p is the volume of a particle of size r defined as $4/3\pi r^3$. The other moments are defined as in equations (11) to (15). Note that the system of moments is closed for these simple kinetics.

$$\frac{\partial}{\partial t}\lambda_{N1} = \sum_{l=1}^{j_{cr}-1}\sum_{i=1}^{2} le_i^l p_{wi}\frac{[P_w^l]}{V_pN_A} + \overline{k}_p[M_{pj}]\lambda_{N0} - \overline{k}_{tr}[M_{pj}]\lambda_{N1} - \overline{k}_{trcta}[CTA_p]\lambda_{N1} - \overline{k}_t\lambda_{N0}\lambda_{N1} \quad (11)$$

$$\frac{\partial}{\partial t}\lambda_{N2} = \sum_{l=1}^{j_{cr}-1}\sum_{i=1}^{2} l^2e_i^l p_{wi}\frac{[P_w^l]}{V_pN_A} + \overline{k}_p[M_{pj}](2\lambda_{N1} + \lambda_{N0}) - \overline{k}_{tr}[M_{pj}]\lambda_{N2} - \overline{k}_{trcta}[CTA_p]\lambda_{N2} - \overline{k}_t\lambda_{N0}\lambda_{N2} \quad (12)$$

$$\frac{\partial}{\partial t}\lambda_{D0} = \overline{k}_{tr}[M_{pj}]\lambda_{N0} + \overline{k}_{trcta}[CTA_p]\lambda_{N0} + (k_{tc}/2 + k_{td})\lambda_{N0}^2 \quad (13)$$

$$\frac{\partial}{\partial t}\lambda_{D1} = \overline{k}_{tr}[M_{pj}]\lambda_{N1} + \overline{k}_{trcta}[CTA_p]\lambda_{N1} + \overline{k}_t\lambda_{N0}\lambda_{N1} \quad (14)$$

$$\frac{\partial}{\partial t}\lambda_{D1} = \overline{k}_{tr}[M_{pj}]\lambda_{N2} + \overline{k}_{trcta}[CTA_p]\lambda_{N2} + \overline{k}_t\lambda_{N0}\lambda_{N2} + k_{tc}\lambda_{N1}^2 \quad (15)$$

The number-average chain length (NACL) and the weight-average chain length (WACL) are defined in equations (16) and (17), respectively:

$$NACL(r,t) = \frac{\lambda_{D1}(r,t)}{\lambda_{D0}(r,t)} \quad (16)$$

$$WACL(r,t) = \frac{\lambda_{D2}(r,t)}{\lambda_{D1}(r,t)} \quad (17)$$

As a further step, since a copolymer system is being modelled, a measure of the copolymer composition is necessary to determine the average molecular weight. The instantaneous copolymer composition corresponding to type i monomer units (I_i) is given by equation (18) and equation

(19):[31,36]

$$I_1 = \frac{f_1(rr_1 f_1 + f_2)}{f_1(rr_1 f_1 + f_2) + f_2(rr_2 f_2 + f_1)} \quad (18)$$

$$I_2 = 1 - I_1 \quad (19)$$

where rr_i is the reactivity ratio and f_i is the mole fraction of monomer i in the particle phase.

The number-average molecular weight (NAMW) in each particle size class is given in equation (20):

$$NAMW(r,t) = (I_1 MW_1 + I_2 MW_2) NACL(r,t) \quad (20)$$

and similarly, the weight-average molecular weight is given by equation (21):

$$WAMW(r,t) = (I_1 MW_1 + I_2 MW_2) WACL(r,t) \quad (21)$$

The global number-average molecular weight, *(Nglob)* and the global weight-average molecular weight, *(Wglob)* for the entire system, are defined in equation (22) and (23), respectively:

$$Nglob(r,t) = \frac{\int_{r_{\min}}^{r_{\max}} NAMW(r,t)\lambda_{D0}(r,t)F(r,t)dr}{\int_{r_{\min}}^{r_{\max}} \lambda_{D0}F(r,t)dr} \quad (22)$$

$$Wglob(r,t) = \frac{\int_{r_{\min}}^{r_{\max}} WAMW(r,t)\lambda_{D1}(r,t)F(r,t)dr}{\int_{r_{\min}}^{r_{\max}} \lambda_{D1}F(r,t)dr} \quad (23)$$

3 Results & Discussion

3.1 Semi-batch Emulsion Polymerisation Simulation: PSD Results

A semi-batch copolymerisation of vinyl acetate (VAc) and butyl acrylate (BuA) was simulated with input trajectories as shown in Figure 1. VAc, BuA and CTA are fed at constant flow rates of 6×10^{-4} and 3×10^{-4} and 1×10^{-4} mol/s, respectively. The initiator is potassium persulphate, surfactant is sodium dodecyl sulphate (SDS) and the CTA is dodecyl mercaptan. The initiator, surfactant and CTA are fed in as aqueous solutions. Model parameters are listed in the appendix. Figure 2 presents the PSD simulation results.

The solution technique used for the PSD model is based on the discretisation of the domain of the internal coordinate into finite elements (FE) or bins. The internal coordinate, taken as particle radius, is equally divided into 250 bins of 2 nm resolution. The representative value for r that is used in PSD calculations is taken to be the mid-point of the bin and a constant particle density is assumed over each bin. The solution algorithm, called the hierarchial two-tier algorithm, is essentially a decomposition algorithm that solves for the nucleation, growth and coagulation phenomena in an individual manner. This decomposition algorithm enables considerable pre-processing, thereby providing very effective computation. See[37,38] for more details on the algorithm.

3.1.1 PSD and the Effects of Nucleation, Growth and Coagulation

A bimodal PSD is generated in this semi-batch operation as shown in Figure 2a. There are no micelles early on in the process ($t < 1s$) as the surfactant concentration is below the critical micelle concentration (cmc) as shown in Figure 2b. Homogenous nucleation takes place at very early times (see Figure 2c) and the resultant mode of particles is seen in Figure 2a (large peak centred around 30 nm). The particles generated by the first homogenous nucleation event are seen clearly in Figure 2d. The homogenous nucleation results in a drop in surfactant concentration (see Figure 2b), which is due to surfactant molecules adsorbing onto the surface of the newly formed particles. The homogenous nucleation dies off due to the entry of the aqueous phase oligomers into the existent particles, rather than achieving the critical chain length.

Due to an increase in the surfactant feed rate as seen in Figure 1, the surfactant

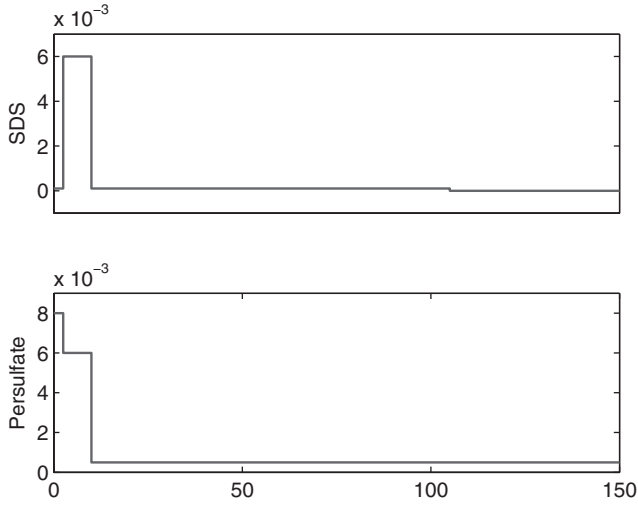

Figure 1.
Simulation base case input flow rates.

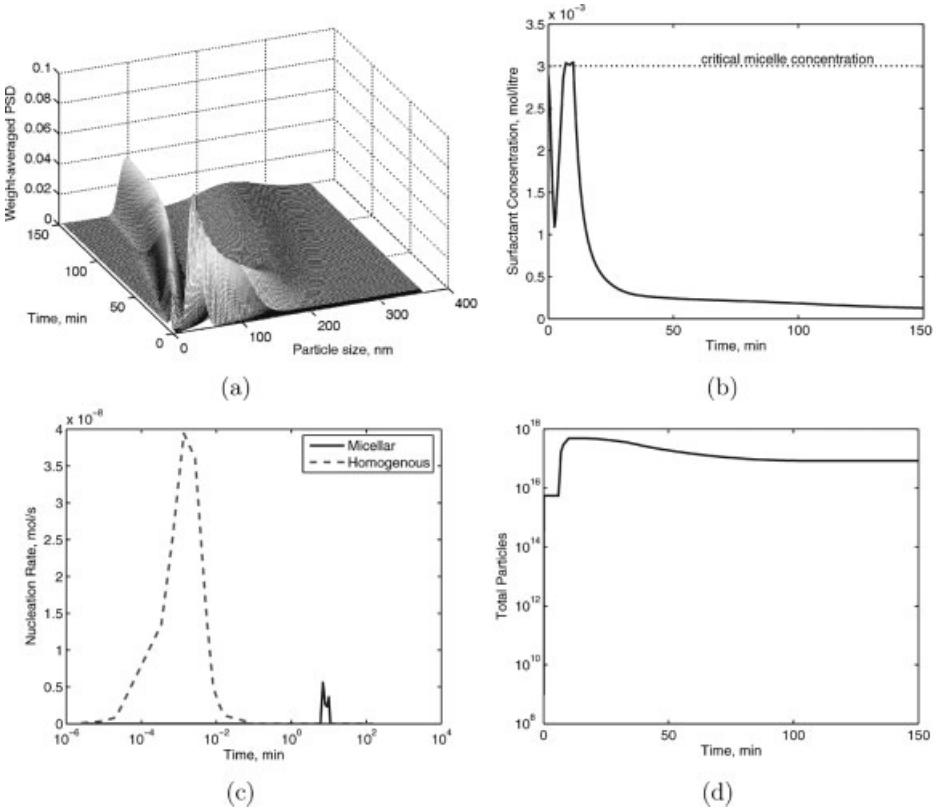

Figure 2.
PSD evolution and the corresponding trends of surfactant concentration, nucleation rates and particle number.

concentration exceeds the cmc at around 10 minutes (see Figure 2b). This results in the micellar nucleation seen in Figure 2c causing the appearance of a bimodal distribution. This results in a fairly steep increase in the number of particles as indicated by Figure 2d, between 10^0 and 10^2 minutes. Following the micellar nucleation of the second mode of particles the surfactant level drops rapidly as it is absorbed by the newly formed particles.

The secondary nucleation of the large number of particles results in a drop in the particle growth rates. This is partly due to the partitioning of the monomers among a large number of particles, and hence a drop in the particle-phase monomer concentration. Another reason for the drop in growth rates is due to a decrease in the average number of radicals per particle, as will be seen in Section 3.1.2. The drop in the surfactant concentration that follows the second nucleation results in reduced particle stabilisation, as evident by the drop in the total particles seen in Figure 2d, due to coagulation. The coagulation kernel is modeled using the Derjaguin-Landau-Verwey-Overbeek (DLVO) theory and is sensitive to the surfactant and initiator concentration. The total net interaction potential is used to calculate the Fuch's stability ratio and hence the coagulation rate between different sized particles.

3.1.2 PSD and Average Number of Radicals/ Particle

The average number of radicals per particle, $\overline{n}(r,t)$ is highly size dependent where larger particles have larger values of $\overline{n}(r,t)$. This size-dependence is related to the rates of entry and termination. Larger particles have larger entry rates, attributed to the collision entry model with entry rates proportional to the square of the particle radius.[33] The termination rate also exhibits size-dependence, with the termination rate decreasing with increase in particle size. The rate of desorption has a reduced size-dependence compared to the rates of entry and termination. Figure 3 shows results to examine the pseudo-bulk vs. zero-one compartmentalisation expected for the system under investigation. Figure 3a shows that the ratio of entry rate to termination rate remains above unity. Referring to Figure 3b one notices that the value of the global average number of radicals (see equation (3)) always assumes a fairly high value and does not drop below 1 except at very early times. One could therefore argue that pseudo-bulk kinetics best describe this system. However the effect of $\overline{n}$ and its inherent assumptions on the evolution of PSD and MWD will be examined further in the forthcoming section.

A final comment is due on the time variation of the average number of radicals per particle. It is seen that $\overline{n}$ and global $\overline{n}$ values increase to very large values at the early times (before about 10 minutes). This is due to the small number of particles formed by the initial homogenous nucleation and hence the net entry of oligomers into each particle is high. Subsequent to the micellar nucleation at around 10 minutes, the large increase in the number of particles leads to reduced entry rates into any given particle, resulting in a net drop in the $\overline{n}$ values (both at the single-particle scale and the global scale).

3.2 MWD Results

In order to solve the partial differential equations representing the live and dead moments given in Section 2.3, a discretisation grid is chosen similar to the one used in the PSD model solution. The grid equally divides the entire particle size domain into discrete bins. Within each bin a representative particle size is chosen (mid-point). The MWD model is formulated focussing on a single particle and so, using the representative particle size, a separate set of moments can be derived for each bin (250 bins). This results in a system of ordinary differential equations, which are solved in combination with the PSD model within a hierarchical two-tier algorithm.[37] At each time step, the PSD model is solved first and then the MWD moment equations -that depend on the PSD- are integrated.

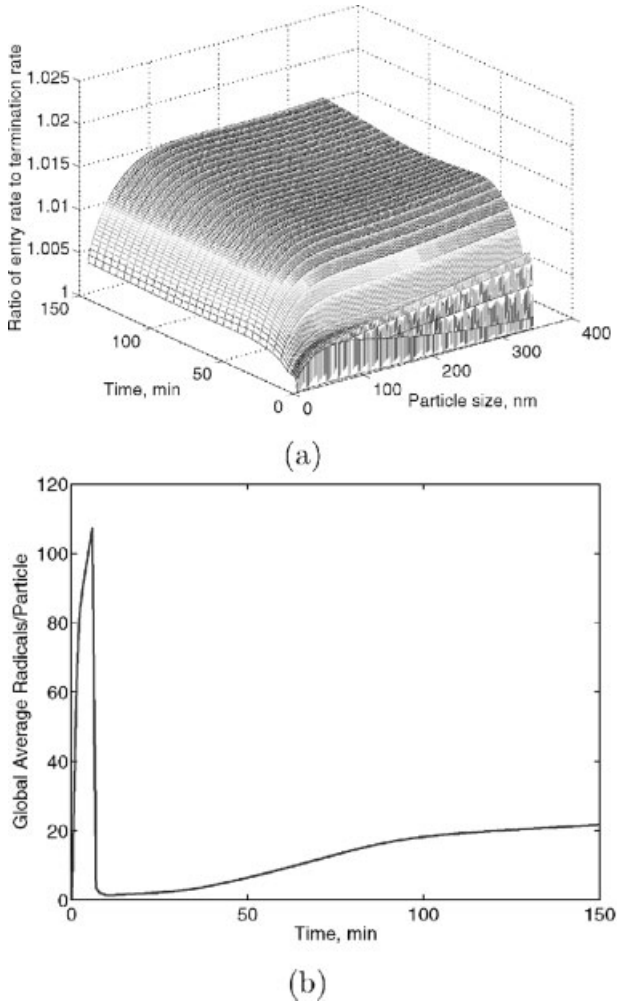

Figure 3.
The ratio of entry to termination and the global average number of radicals/particle.

Fast kinetics are assumed to describe the live chains, therefore a pseudo-steady state is applied. So the effect of particle growth is unimportant in solving the live radical moments. However, neglecting particle growth effects could lead to widely different model predictions for the dead chain moments, as will be shown later. This makes it important to account for growth in solving the dead chain moment balances. This is done by setting the initial condition of the dead chain moments at the start of a discrete time step in a particular bin equal to the value at the end of the previous time step in a preceding bin as determined by the growth rates. This will require the initial condition of the dead chain moments in the first bin to be set to zero. The method is again a sequential decomposition algorithm that builds the population-level behavior by examining individual particle behaviors.

3.2.1 Semi-batch Simulation Results

A semi-batch simulation produced the following MWD plots (see Figures 4–5).

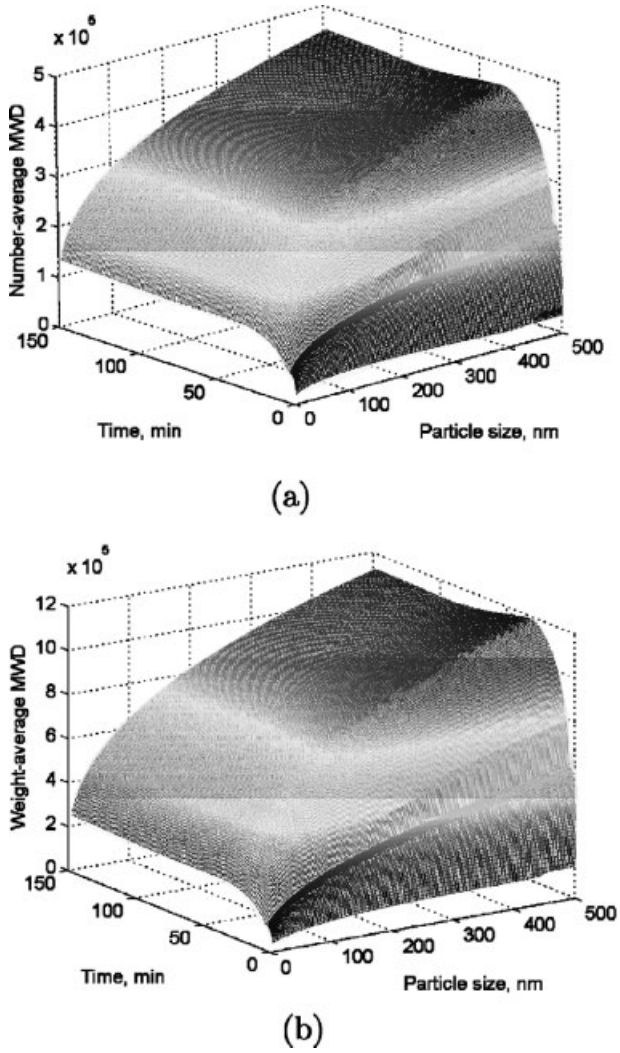

Figure 4.
Number-average and weight-average MWD evolution.

Figure 4 indicates a size-dependence and time evolution of the average molecular weight.

Figures 4a and 4b show that MWD increases with time for approximately the first 40 minutes of reaction, after which little increase in MWD is observed. The same figures also elucidate the distinct size dependance of the MWD in both the number-average and weight-average cases. The molecular weight increases with increasing particle size. This can be associated with the increased chance that radicals have to grow via propagation reactions in large particles, until they undergo any of the other reactions (e.g. termination, chain transfer) which lead to cessation of growth. The global average molecular weights are shown in Figure 5, which exhibit a similar time evolutionary trend to that observed for the distribution evolutions; during the first 40 minutes a rapid increase in molecular weight is observed, after which there is a very gradual increase, reaching a

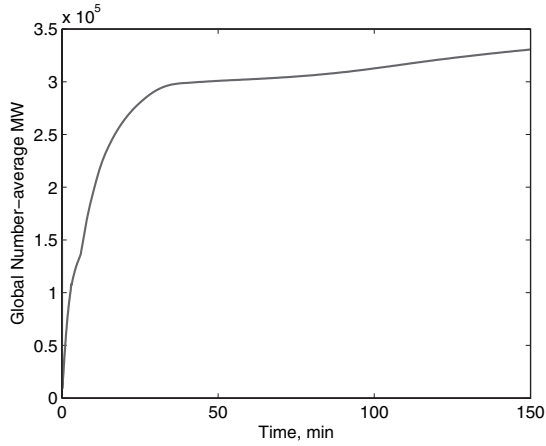

(a)

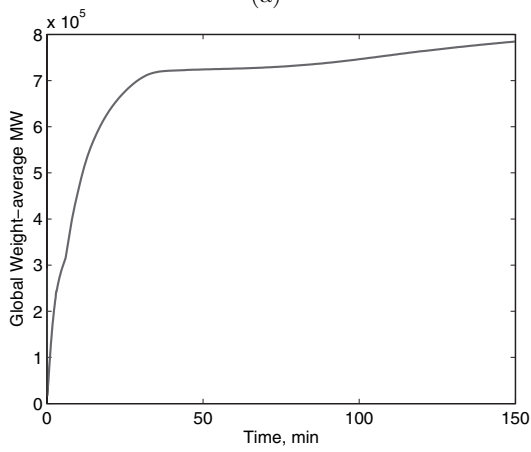

(b)

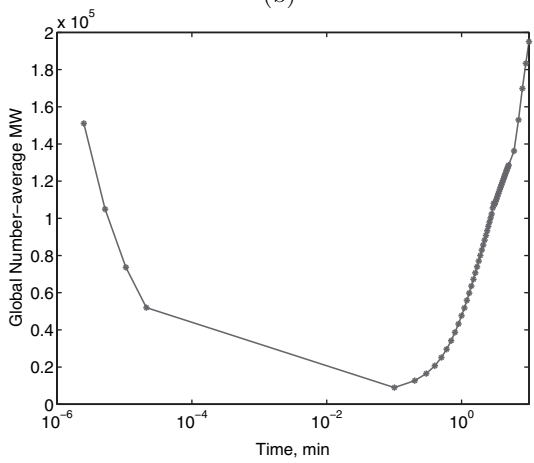

(c)

Figure 5.
Global number-average and global weight-average MW evolution and an initial time plot of the global number-average MW evolution.

number-average molecular weight value of approximately 300,000. The behavior at very early times is indicated in Figure 5c for the global number-average molecular weight. It is seen that there is an initial jump in the average molecular weight followed by a decrease as homogenous nucleation occurs and as more polymer chains are initiated. A similar trend is observed at early times in the distribution plots (not included in Figure 4 for clarity). As homogenous nucleation is completed, the average molecular weight begins to increase.

As discussed previously, the increase is monotonic after this time, except for a momentary decrease in growth rates between 7–10 minutes, when the second micellar nucleation event is underway.

3.2.2 Effect of Particle Growth on MWD

As stated previously in Section 3.2, it is assumed that fast kinetics govern the live radicals, therefore a pseudo-steady state is applied to the live radical balances. The effect of growth by polymerisation inside particles need not be accounted for as far as the live radicals are concerned. However, the same is not true for dead polymer chains, the kinetics of which are assumed to be far slower. For this reason the differential form of the dead chain balances is retained and also the effect of growth will need to be accounted for in the model of dead polymer chains. It is of interest to study the relative importance of including growth dynamics on the MWD predictions, so as to explore the possibility of model simplifications. Figure 6 shows the effect of accounting for growth in the MWD model. The growth effect can be seen to cause a prolonged initial increase in the both the global average molecular weights. This results in a higher eventual molecular weight value than would have been predicted based on neglecting growth. For the global number-average molecular weight, an increase of approximately 100% is seen when growth is accounted for. In the case of global weight-average molecular weight, an increase of approximately 25% is observed. These results illustrate the importance of accounting for the particle growth from the PSD model in the MWD model.

3.3 Effect of Compartmentalisation on Termination Rates: Sensitivity on PSD and MWD

A factor f was introduced into equation (2) with the intent of evaluating the sensitivity of the model objectives (PSD and MWD) to variations in bimolecular termination.[22] The factor serves to reduce the level of termination in particles and assumes values in the range 0.2 (20% termination) to 1 (full termination). In particles with a small number of radicals, compartmentalisation governs the amount of bimolecular termination, so by observing the effect of varying the termination rate within particles one can assess the impact of the compartmentalisation phenomena on the process.

$$\frac{\partial \overline{n}}{\partial t}(r,t) = \Re_{entry}(r) - \Re'_{desorp}\overline{n}(r) - f2\Re'_{termin}\overline{n}^2(r) \quad (24)$$

It is seen in Figure 7a that the global average number of radicals per particle increased as the factor f was decreased. The reduction in termination means that the net effect of entry is made stronger as depicted in Figure 7a. This in turn results in larger growth rates and hence larger particle sizes as is seen in Figure 7b. The net effect on the molecular weight is seen in Figure 8. With a reduction in termination, lower global average molecular weights are observed. When the termination is reduced by 40% (from 100% to 60%) the end molecular weight that is achieved is approximately 20% lower. When the termination is reduced by a further 20% (from 60% to 40%), the end molecular weight is reduced by approximately 20%. Finally, when the termination is reduced by a further 20% (from 40% to 20%) the end molecular weight is reduced by approximately 35%. These approximate values indicate a non-linear relation between the termination factor and molecular weight. It is clear from the results that the decrease in termination

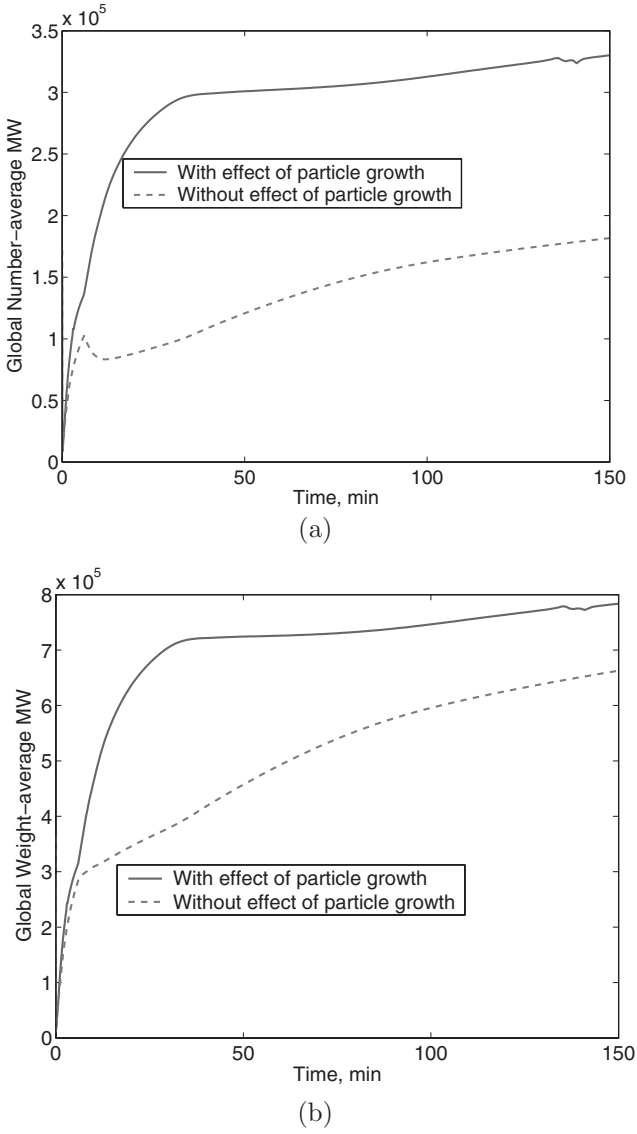

Figure 6.
Global average molecular weight evolutions analysing the effect of particle growth.

rate plays a more important role in determining the molecular weights than on any other cascaded effects of a reduction in *f*.

3.4 Macroscopic Process Sensitivities to Process Manipulations

The flow rates of important process inputs were perturbed from the nominal values shown in Figure 1. In the case of monomer flow rates, both VAc and BuA were changed in equal ratio. Figure 9a indicates that increasing monomer flow rates by 20% increases the MWD. Whilst increasing the monomer would lead to more aqueous oligomers, hence entry of small chains into particles lowering the average molecular weight, the effect of a larger monomer concentration in particles has a stronger effect. This leads to a higher polymerisation rate of chains inside particles, hence

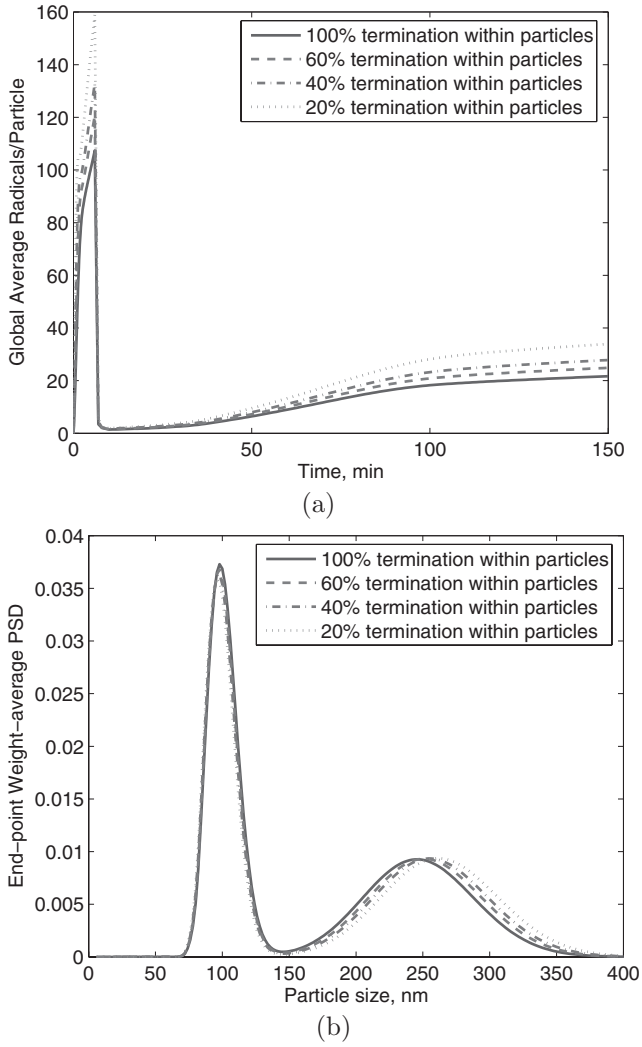

Figure 7.
The effect of introducing a termination correction factor in the calculation of $\overline{n}$ on the global average number of radicals per particle and the end-point PSD.

increasing the average chain length. Lowering the monomer flow rate results in a lower concentration in particles and has the opposite effect, lowering the molecular weights. Figure 9b indicates that increasing monomer flow rate results in a shift of all modes of particles to the right, due to increased growth rates. It also shows the general trend of peaks shifting to left when monomer flow rate is decreased, due to decreased growth rates. If one focusses on the mode of particles centred around about 250 nm (homogeneously nucleated), upon increasing monomer flow rate this peak shifts up due to increased monomer concentration and hence growth. The opposite movement is observed upon decrease in monomer flow rate. There seems to be little change in the number of particles contained in this mode, which means that there is no alteration in the homogenous nucleation rate, despite the increased aqueous phase monomer concentration. This points to the fact that the initiation of monomer maybe

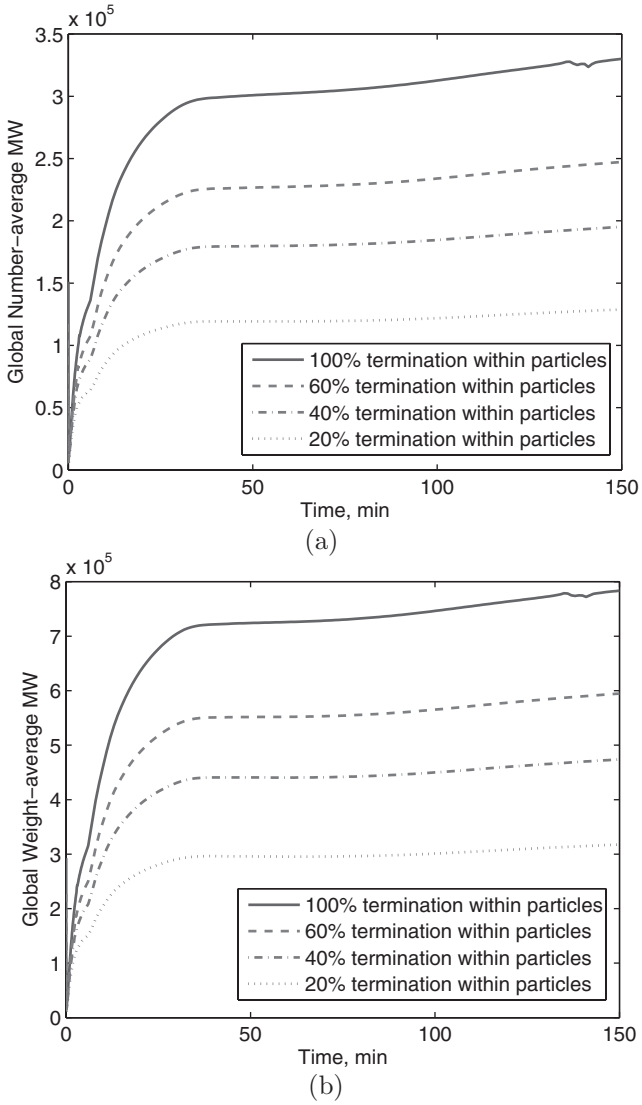

Figure 8.
The effect of introducing a termination correction factor in the calculation of $\overline{n}$ on the global average molecular weight evolutions.

the limiting factor in this case. In the case where the monomer flow rate is increased, there is an initial period of increased growth of the homogenously nucleated particles. These growing particles adsorb more surfactants onto their surfaces, resulting in less monomer being available for the subsequent micellar nucleation, observed in the smaller peak centred around about 110 nm.

An increase in surfactant flow rate results in a small increase in MWD (not shown). The increased surfactant level leads to an increased micellar nucleation, which leads to larger overall number of particles. This results in a decreased value of the global average number of radicals/particle. With less radicals to terminate inside a particle, polymerisation occurs for

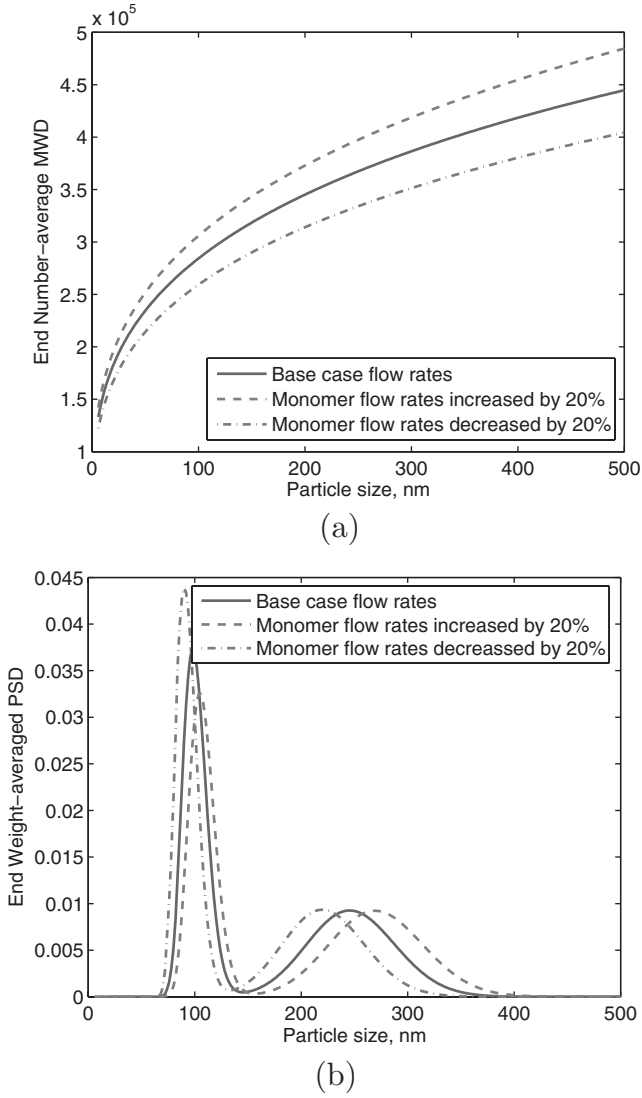

Figure 9.
The effect of perturbations in monomer flow rates on end-time PSD and MWD.

longer and at higher propagation rates, therefore higher molecular weights are observed. A decrease in surfactant level results in a higher number of radicals/particle on average and lower molecular weights are observed. The effect of perturbations in surfactant flow rate on the end-time PSD is to alter the relative sizes and position of the two modes of particles. The amount of homogenous nucleation that occurs at the start of the process is the same in the different cases. In the increased surfactant case, the base case homogenously nucleated peak becomes slightly smaller and shifts to the left due to a decreased level of growth subsequent to the larger micellar nucleation. When the surfactant level is decreased the converse effect is observed.

Persulfate perturbations lead to different trends to those seen previously. As initiator flow rate is increased, MWD

decreases. This effect is due to the increased concentration of aqueous phase oligomer. The increased entry rate of oligomers into particles has a negative effect on MWD. A decrease in initiator flow rate has the opposite effect. The effect of initiator perturbations on PSD is explained as follows: as the initiator flow rate is increased the level of aqueous phase oligomers increases, resulting in a larger homogenously nucleated peak. Therefore, the subsequent micellar nucleation is smaller (resulting in a smaller peak). Decreasing the initiator flow rate results in a smaller homogenously nucleated peak and a larger micellar nucleation.

The effect of perturbations to CTA flow rates is seen in Figure 10. With respect to the MWD plot in Figure 10a, an increase in CTA flow rate results in a decrease in MWD, as expected. If CTA is not used in the process, then radicals within particles

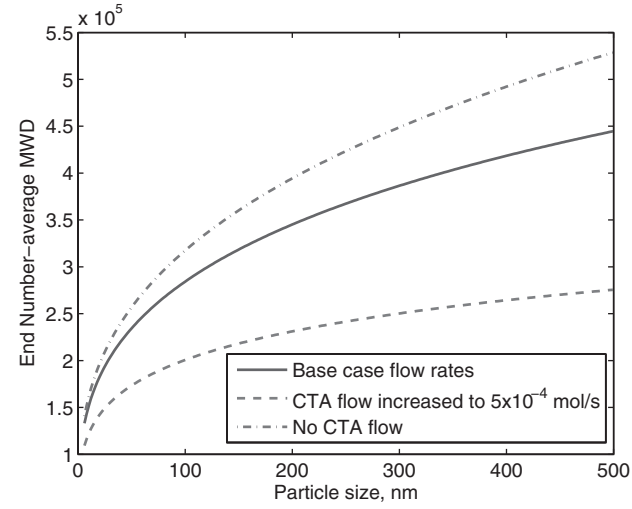

(a)

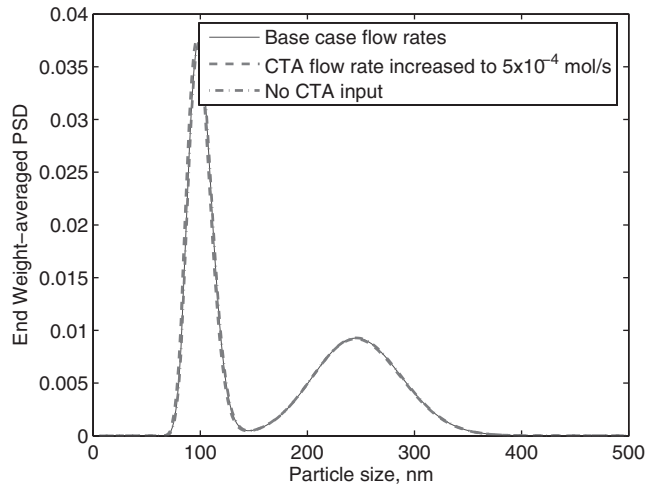

(b)

Figure 10.
The effect of perturbations in CTA flowrate on end-time PSD and MWD.

are more likely to achieve longer chain lengths, resulting in a higher MWD. Figure 10b indicates that CTA perturbations have negligible effect on PSD development. This result demonstrates that CTA provides the mechanism to manipulate MWD, without altering the PSD, leading to a more flexible control regime. Although a mechanism exists for the MWD to influence the PSD, for example by the desorption of radicals from particles, the point to note with the analysis presented here is the insignificance of that mechanism.

4 Conclusions

This paper details a preliminary version of a comprehensive model that simultaneously accounts for both PSD and MWD. The results of a semi-batch emulsion polymerisation simulation elucidate the effect of process variables and model parameters on PSD and MWD. The MWD was shown to be highly size dependent, where larger average molecular weights were seen in larger particles. A decomposition solution technique called the hierarchial two-tier algorithm is employed for the solution of the combined model. The solution technique resulted in a computational time of approximately 40 seconds (for a 150 minute semi-batch process) on a contemporary computer, consisting of a dual core 3.4 GHz Intel pentium D processor with 1 GB of memory. The sensitivity of the objectives of PSD and MWD was assessed in relation to perturbations in monomer, surfactant, initiator and CTA inputs. The largest effects on MWD were seen in the cases of varying monomer, initiator and CTA. CTA offered the possibility of manipulating MWD, without changing PSD. The main points to be taken from the analysis of the effect of compartmentalisation on the process objectives is that PSD is little affected, however a larger effect was noted with respect to the MWD. Therefore, this effect needs to be modified in future, to improve model predictive capabilities. Having elucidated the effects of compartmentalisation, in a forthcoming version of this combined model it is envisioned to include an appropriate modification to the termination events within the particles. This will be done with an aim to dynamically adapt the termination kinetics in the range spanned between zero-one and pseudo-bulk regimes.

Appendix 1: Sample derivation for moment equations

The first moment of the live radical balance is derived as follows: Summing the contributions from individual equations for live radicals:

$$\begin{aligned}\frac{\partial}{\partial t}\lambda_{N_1}(r,t) &= \frac{\partial}{\partial t}\sum_{l=0}^{\infty} lN^1(r,t) = \frac{\partial}{\partial t} lN^0(r,t) \\ &+ \frac{\partial}{\partial t}\sum_{l=1}^{j_{cr}-1} lN^1(r,t) \\ &+ \frac{\partial}{\partial t}\sum_{l=j_{cr}}^{\infty} lN^1(r,t) \end{aligned} \quad (25)$$

Considering the contributions from individual rates to equation (25),

$$\begin{aligned}\frac{\partial}{\partial t}\lambda N_1 = \Re'_{entry} + \Re'_{prop} + \Re'_{tr} + \Re'_{trcta} \\ + \Re'_{termin} + \Re'_{desorp}\end{aligned} \quad (26)$$

where $\Re'_{entry}$ is the rate contribution from particle entry events, $\Re'_{prop}$ is the rate contribution from propagation, $\Re'_{tr}$ is the rate contribution from chain transfer to monomer, $\Re'_{trcta}$ is the rate contribution from chain transfer to CTA, $\Re'_{termin}$ is the rate contribution from termination within a particle and $\Re'_{desorp}$ is the rate contribution from desorption from a particle. These rate term are derived as follows:

$$\Re'_{entry} = \sum_{l=1}^{j_{cr}-1}\sum_{i=1}^{2} le_i^l p_{wi}[p_w^l]/V_p N_A \quad (27)$$

$$\begin{aligned}\Re'_{propagation} &= \overline{k}_p[M_{pj}]N^0 l + \sum_{l=1}^{\infty} l\overline{k}_p[M_{pj}](N^{l-1} - N^l) \\ &= \overline{k}_p[M_{pj}]\left[\sum_{l=1}^{\infty} l(N^{l-1}) - \sum_{l=1}^{\infty} lN^l\right] \\ &= \overline{k}_p[M_{pj}]\left[(N^0 + 2N^1 + 3N^2 \ldots) - (N^1 + 2N^2 \ldots)\right] \\ &= \overline{kp}[M_{pj}]\left[(N^0 + N^1 + N^2 ..)\right] \\ &= \overline{k}_p[M_{pj}]\lambda_{n0}\end{aligned} \tag{28}$$

$$\begin{aligned}\Re'_{ct} &= \overline{k}_{tr}[M_{pj}](\lambda_{N0} - N^0)l - \sum_{l=1}^{\infty} \overline{k}_{tr}[M_{pj}]N^l l \\ &= -\overline{k}_{tr}[M_{pj}]\left[0N^0 + \sum_{l=1}^{\infty} lN^l\right] \\ &= -\overline{k}_{tr}[M_{pj}][0N^0 + 1N^1 + 2N^2 \ldots] \\ &= -\overline{k}_{tr}[M_{pj}]\lambda_{N1}\end{aligned} \tag{29}$$

$$\begin{aligned}\Re'_{trcta} &= \overline{k}_{trcta}[CTA_p](\lambda_{N0} - N^0)l - \sum_{l=1}^{\infty} \overline{k}_{tr}[M_{pj}]N^l l \\ &= -\overline{k}_{trcta}[CTA_p]\left[0N^0 + \sum_{l=1}^{\infty} lN^l\right] \\ &= -\overline{k}_{trcta}[CTA_p][0N^0 + 1N^1 + 2N^2 \ldots] \\ &= -\overline{k}_{trcta}[CTA_p]\lambda_{N1}\end{aligned} \tag{30}$$

$$\begin{aligned}\Re'_{ter\ mination} &= -\overline{k}_t N^0 \lambda_{N0} l - \sum_{l=1}^{\infty} \overline{k}_t N^l \lambda_{N0} l \\ &= -\overline{k}_t \lambda_{N0}\left[0N^0 + \sum_{l=1}^{\infty} lN^l\right] \\ &= -\overline{k}_t \lambda_{N0}\left[\sum_{l=0}^{\infty} lN^l\right] \\ &= -\overline{k}_t \lambda_{N0}\lambda_{N1}\end{aligned} \tag{31}$$

$$\Re'_{desorbtion} = \sum_{j=1}^{2} k_{dnj} p_j N^0 l = 0 \tag{32}$$

Giving the first moment of the live radical balance:

$$\frac{\partial}{\partial t}\lambda_{N1} = \sum_{l=1}^{j_{cr}-1}\sum_{i=1}^{2} le_i^l p_{wi}[p_w^l]/V_p N_A + \overline{k}_p[M_{pj}]\lambda_{n0} - \overline{k}_{tr}[M_{pj}]\lambda_{N1} - \overline{k}_{trcta}[CTA_p]\lambda_{N1} - \overline{k}_t\lambda_{N0}\lambda_{N1} \tag{33}$$

Appendix 2: Simplifications

Pseudo-homopolymer Rate Constants

$$\begin{array}{ll} \overline{k}_p = \sum_{i=1}^{2}\sum_{j=1}^{2} k_{pij} p_i p_j & \overline{k}_t = \sum_{i=1}^{2}\sum_{j=1}^{2} (k_{tcij} + k_{tdij}) p_i p_j \\ \overline{k}_{tr} = \sum_{i=1}^{2}\sum_{j=1}^{2} k_{trij} p_i p_j & \overline{k}_{tc} = \sum_{i=1}^{2}\sum_{j=1}^{2} (k_{tcij}) p_i p_j \\ \overline{k}_{trcta} = \sum_{i=1}^{2} k_{trcta,iPi} & \overline{k}_{td} = \sum_{i=1}^{2}\sum_{j=1}^{2} (k_{tdij}) p_i p_j \end{array} \tag{34}$$

Appendix 3: Nomenclature

r	particle radius
$F(r, t)$	particle density function
$\Re_{coag}$	rate of particle coagulation
$\Re_{nuc}$	rate of particle nucleation
$\overline{n}$	average number of radicals per particle
$\overline{n}_{global}$	global average number of radicals per particle
$\Re_{entry}$	total rate of entry into a particle
$\Re_{ter\ min}$	total rate of termination within a particle
$\Re_{desorp}$	total rate of desorption from a particle
N^l	concentration of live radicals of length l in the particle phase
D^l	concentration of dead polymer chains of length l in the particle phase
e_i^l	entry rate constant for an aqueous oligomer of length l and type i
p_i	probability that a radical is of type i (particle phase)
p_{wi}	probability that a radical is of type i (aqueous phase)
M_{pj}	moles of monomer of type j (particle phase)
CTA_p	moles of CTA (particle phase)
$\mathrm{V_p}$	volume of a polymer particle
j_{cr}	critical chain length
k_{pij}	propagation constant for type i polymer with type j monomer (particle phase)
k_{trij}	chain transfer constant from type i polymer to type j monomer (particle phase)
$k_{trcta,i}$	chain transfer constant from type i polymer to CTA (particle phase)
k_{tij}	termination constant between type i and j radicals (particle phase)
k_{tcij}	combination termination constant between type i and type j radicals (particle phase)
K_{tdij}	disproportionation termination constant between type i and type j radicals (particle phase)
k_{dnj}	desorption constant for monomeric radicals of type j
λ_{Nk}	k^{th} moment of the live radical population balance
λ_{Dk}	k^{th} moment of the dead polymer population balance
NACL	number-average chain length
WACL	weight-average chain length
NAMW	number-average molecular weight
WAMW	weight-average molecular weight
I_i	instantaneous copolymer composition corresponding to type i monomer units
N_{glob}	global number-average molecular weight
W_{glob}	global weight-average molecular weight
rr	reactivity ratio

Appendix 4: Kinetic and physical parameter values

k_{p11}	3.29×10^3 L/mol · s	$k_{tr11} = k_{tr12} = k_{tr21} = k_{tr22}$	9.3×10^{-3} L/mol · s
k_{p12}	8.9×10^4 L/mol · s	k_{t11}	1.05×10^7 L/mol · s
k_{p21}	3.9×10^1 L/mol · s	k_{t22}	1.6×10^3 L/mol · s
k_{p22}	2.47×10^2 L/mol · s	$k_{trcta,1} = k_{trcta,2}$	1×10^0
cmc	3.0×10^{-3} mol/L	MW_{surf}	288.5
$MW_{initiator}$	238	j_{cr}	5

[1] C. Parkinson, S. Matsumoto, P. Sherman, *J. Colloid Interface Sci.* **1970**, *33*, 150.
[2] P. F. Luckham, M. A. Ukeje, *J. Colloid Interface Sci.* **1999**, *220*, 347.
[3] R. W. Nunes, J. R. Martin, J. F. Johnson, *Polym. Eng. Sci.* **1982**, *22*, 205.
[4] J. E. Puskas, P. Chan, K. B. McAuley, G. Kaszas, S. Shaikh, *Polymer Reaction Engineering VI conference* **2006**, Halifax, Canada, May.
[5] W. H. Smith, R. H. Ewart, *J. Chem. Phys.* **1948**, *16*, 592.
[6] K. W. Min, W. H. Ray, *J. Macromol. Sci., Rev. Macromol. Chem. Phys.* **1974**, *2*, 177.
[7] J. Rawlings, W. H. Ray, *Polym. Eng. Sci.* **1988a**, *28*, 237.
[8] J. Rawlings, W. H. Ray, *Polym. Eng. Sci.* **1988b**, *28*, 257.
[9] S. Chen, K. Wu, *J. Polym. Sci., Part A: Polym. Chem.* **1988**, *26*, 1487.

[10] G. Storti, S. Carra, M. Morbidelli, G. Vita, *J. Appl. Polym. Sci.* **1989**, *37*, 2443.
[11] E. M. Coen, R. G. Gilebrt, B. R. Morrison, H. Leube, S. Peach, *Polymer* **1998**, *39*, 7099.
[12] E. Saldívar, P. Dafiniotis, H. Ray, *J. Macromol. Sci., Rev. Macromol. Chem. Phys.* **1998**, *27*, 403.
[13] T. Crowley, E. Meadows, E. Kostoulas, F. J. Doyle III, *J. Process Contr.* **2000**, *10*, 419.
[14] P. H. H. Araujo, J. C. de la Cal, J. M. Asua, J. C. Pinto, *Macromol. Theory Simul.* **2001**, *10*, 769.
[15] J. Zeaiter, J. A. Romagnoli, G. W. Barton, V. G. Gomes, B. S. Hawkett, G. R. G. , *Chem. Eng. Sci.* **2002**, *57*, 2955.
[16] E. Ginsburger, F. Pla, C. Fonteix, S. Hoppe, S. Massebeuf, P. Hobbes, P. Swaels, *Chem. Eng. Sci.* **2003**, *58*, 4493.
[17] E. L. Casella, O. Araujo, R. Giudici, *Polym. React. Eng.* **2003**, *11*, 869.
[18] E. Saldivar, O. Araujo, R. Giudici, *J. Appl. Polym. Sci.* **2002**, *84*, 1320.
[19] O. Araujo, R. Giudici, E. Saldivar, *J. Appl. Polym. Sci.* **2001**, *79*, 2360.
[20] A. F. Santos, E. L. Lima, J. C. Pinto, *J. Appl. Polym. Sci.* **2003**, *90*, 1213.
[21] M. F. Heredia, M. Schneider, C. Graillat, T. McKenna, *Macromol. Symp.* **2000**, *150*, 95.
[22] E. Giannetti, G. Storti, M. Morbidelli, *J. Polym. Sci., Part A: Polym. Chem.* **1988**, *26*, 2307.
[23] G. Storti, G. Polotti, P. Canu, M. Morbidelli, *J. Polym. Sci., Part A: Polym. Chem.* **1992**, *30*, 751.
[24] G. Arzamendi, J. Forcada, J. M. Asua, *Macromolecules* **1994**, *27*, 6068.
[25] L. Vallermaux, *J. Blavier, Chem. Eng. Sci.* **1984**, *39*, 87.
[26] G. Arzamendi, C. Sayer, N. Zoco, J. M. Asua, *Polym. React. Eng.* **1998**, *6*, 193.
[27] C. Sayer, P. H. H. Arajo, G. Arzamendi, J. M. Asua, E. L. Lima, J. C. Pinto, *J. Polym.Sci., Part A: Polym. Chem.* **2001**, *39*, 3513.
[28] G. Lichti, R. G. Gilbert, D. H. Napper, *J. Polym. Sci., Part A: Polym. Chem.* **1980**, *18*, 1297.
[29] A. Ghielmi, G. Storti, M. Morbidelli, W. H. Ray, *Macromolecules* **1998**, *31*, 7172.
[30] A. Butte, G. Storti, M. Morbidelli, *Macromol. Theory Simul.* **2002**, *11*, 37.
[31] M. Park, M. T. Dokucu, F. J. Doyle III, *Macromol. Theory Simul.* **2005**, *14*, 474.
[32] X. E. E. Reynhout, J. Meuldijk, P. D. Iedema, M. Wulkow, *Polym. Plast. Technol. Eng.* **2005**, *44*, 707.
[33] C. D. Immanuel, C. F. Cordeiro, S. S. Sundaram, E. S. Meadows, T. J. Crowley, F. J. Doyle III, *Comput. Chem. Eng.* **2002**, *26*, 1133.
[34] S. Melis, M. Kemmere, J. Meuldijk, G. Storti, M. Morbidelli, *Chem. Eng. Sci.* **2000**, *55*, 3101.
[35] C. D. Immanuel, F. J. Doyle III, C. F. Cordeiro, S. S. Sundaram, *AlChE J.* **2003**, *49*, 1392.
[36] F. R. Mayo, F. M. Lewis, *J. Am. Chem. Soc.* **1944**, *66*, 1594.
[37] C. D. Immanuel, F. J. Doyle III, *Chem. Eng. Sci.* **2003**, *58*, 3681.
[38] N. Sun, C. D. Immanuel, *T. I. Meas. Control* **2005**, *27*, 347.

